LHCb 2002-025 Muon
19 April 2002

Test results of a full size prototype of the muon chambers for region M2/R4 of the LHCb Muon System.

B.Bochin, S.Guets, V.Lazarev, N.Saguidova, E.Spiridenkov, An.Vorobiev, A.Vorobyov

Petersburg Nuclear Physics Institute

Abstract

A full size prototype M2R4-01 of the Wire Pad Chambers for region M2/R4 of the LHCb Muon System has been constructed at PNPI and tested in the T11 beam at CERN. The prototype contained two double-gap chambers with the sensitive area of 25x120 cm^2. Each double-gap chamber contained 24 wire pads of 5x25 cm^2 size. The prototype was fully instrumented with the FE electronics based on SONY chips with active adapters at the input allowing to optimize the parameters of the read out channels. The chamber was tested with four different concentrations of the gas components in the Ar/CO2/CF4 gas mixture. The beam tests showed quite satisfactory performance of the M2R4-01 prototype: a wide efficiency plateau uniform over the whole sensitive area of the chamber, low noise rates and cross-talks. It was demonstrated that the gas mixtures Ar(40%)+CO2(40%,30%)+CF4(20%,30%) provide higher stability against the HV-trips thus extending essentially the operational plateau of the chamber.

1 Introduction

Since 1998, nine different prototypes of the wire pad chambers (WPC) have been constructed at PNPI and tested in the PS beam at CERN [1-3]. This allowed to optimize the WPC design parameters. It was demonstrated that the proposed four-gap WPC can satisfy the requirements of the LHCb Muon System (outer regions) with a solid redundancy. The tested WPC prototypes were equipped with the front-end electronics based on discrete elements. This electronics was designed and constructed at PNPI, and it was optimized according to the requirements of the experiment: low input impedance, low noise at large input capacitance, fast enough output signal with tail cancellation. In addition, a new option of the FE electronics has been developed at PNPI based on the SONY chip with an active adapter at the input of the chip allowing to reduce the input impedance and the width of the shaped signal. This option (SONY++) was tested with the WPC-9 prototype with very satisfactory results [3].

Based on these studies, a full size prototype of the muon chambers for region R4, station M2 has been constructed at PNPI. This prototype (M2R4-01) was fully equipped with the SONY++ FE electronics. It was tested in the T11 beam at CERN in the test runs performed in May and November 2001. Here we report on the results of these tests.

2 Design of the M2R4-01 prototype

The M2R4-01 prototype contains four layers of wire chambers (A, B, C, and D) with the sensitive area of 25x120 cm^2 (Figures 1 to 4).

The inside cathode panels were prepared at PNPI by glueing 1.5 mm thick Cu-cladded FR4 plates to 6 mm thick honeycomb panels. The FR4 plates and the honeycomb panels were purchased with the requirement of the best possible uniformity in the thickness of the material. The measured flatness of thus prepared cathode panels proved to be within ±50μm. The outer cathode panels were made of 3.2 mm thick FR4 plates Cu-cladded on both sides.

The shape of the anode wire fixation bars was similar to that in the WPC-9 prototype (Figure 2). The thickness of the anode bars was (2.45±0,01) mm. The anode bars were glued to the cathode panels with a controllable layer (50 μm) of the epoxy glue. The thickness of the cathode bars (Figure 2), as well as that of the side bars (Figure 3) was also (2.45±0,01) mm, and they were glued to the cathode panels in the same way as the anode bars.

The anode wires of 30 μm in diameter were wound around the cathode planes containing the anode bars. The wire spacing was 1.5mm and the wire tension was 50 g. In addition, two 100 μm guard wires were put at each side of the wire plane. The wires were first glued and then soldered to the anode bars. After that they were cut behind the soldering places thus making the anode planes electrically independent.

The whole stack of the panels was bolted together with the help of 20 studs (4 mm in diameter) uniformly distributed along the perimeter of the chamber. The O-rings provided isolation of the studs from the gas volume (Figure 2). For final gas tightening, an RTV layer was distributed all around the external surface of the bars. The RTV could be easily removed thus allowing (if needed) reassembling the chamber. Figure 3 shows the scheme of the sequential gas flow in the chamber.

The anode wires in each wire plane (A, B, C, and D) were grouped together forming the 49.5 mm wide wire pads. There were 24 wire pads in each plane. One side of each wire pad was connected to a common HV bus through a 1.5 MΩ resistor. The other side of each wire pad was connected through a 1000pF decoupling capacitor to the input of the preamplifier (Figure 4). The opposite wire pads from the neighbour wire planes (A&B and C&D) were connected to one common preamplifier, so the chamber operated in the "two double-gaps" mode, as it is foreseen in the LHCb Muon System. The HV could be regulated independently in each plane. Note that there was no special wire staggering between the wire planes. As it was shown in [1], the staggering is not essential in the chosen wire chamber geometry.

All cathodes were grounded at the read out side in a set of points along the length of the chamber (every 10 cm). Such scheme reduces the currents across the wire pads thus decreasing the possible cross-talks between the wire pads.

Table1. M2R4-01 geometry parameters.

Sensitive area	25x120cm^2
Number of gaps	4 (2 double-layers)
Gap width	5.0 mm
Wire diameter	30 μm.
Wire spacing	1.50 mm.
Wire tension	50 g
Wire pad size	4.95 x 25 cm^2
Total gas volume	6 liters

3 Electronics

The M2R4-1 prototype was fully equipped with the read out electronics. In total, there were 48 read out channels with modified SONY chips (SONY++) as the front-end electronics. The modification of the SONY chip was described in our note [3]. Unfortunately, direct application of the SONY chips as the preamplifiers in the LHCb muon chambers revealed several problems: large input impedance (80 Ω), relatively long output signal (200 ns full width), and not sufficient amplification factor resulted in a worse time resolution, larger cross-talks, and larger dead time in comparison with the PNPI FE electronics (based on discrete elements) used in all our previous tests. In the modified option SONY++, an active adapter was added in front of the SONY chip designed in such a way that the input impedance was reduced to 25 Ω, the amplification factor was increased by a factor of 3, the full length of the output signal was reduced to 60 ns, and the tail cancellation was provided. The SONY++ chips have been tested with the WPC-9 prototype and demonstrated very good performance, identical to that of the PNPI FE electronics.

Each SONY chip contains 4 channels with digital and analog outputs in each channel. The digital signals are produced by the in-chip discriminator with variable threshold and sent through the LVDC->ECL converters to TDCs for time measurements while the analog signals were used for charge measurements. As an illustration, Figure 5 shows the shape of the signal produced by a beam particle at the analog output of the SONY++ chip (WPC-9 prototype, double-gap mode, pad size 8x16 cm^2).

4 Experimental setup in the T11 beam

The tests were carried out at CERN in a 3 GeV/c negative pion beam at PS. The layout of the experiment is shown in Figure 6. The chamber was installed on a moveable platform allowing to vary the beam position over the whole surface of the chamber. The chamber plane was perpendicular to the beam direction. Beam particles were detected with two scintillator counters: S1 (15 cm x 15 cm) and S2 (20 cm x 20 cm). The coincidence between these two counters in a 10 ns window provided a trigger signal: TR1 = S1 x S2.

The constant-fraction discriminators (CFD) were used in both S1 and S2 channels helping to reduce the time jitter of the trigger signal down to ≤1 ns. The beam particles were detected also by two planes (H-horizontal and V-vertical) of the hodoscope counters, each plane containing 8

counters (1 cm x 8 cm). The following information was registered by the acquisition system:

- Time arrivals and amplitudes of the signals from the S1 and S2 scincillator counters measured with TDCs and ADCs.
- Time arrivals of the signals from all hodoscope counters measured with TDCs.
- Time arrivals of the signals from the WPC measured with TDCs.
- Integrated current signals from the WPC measured with ADCs.

In addition, there was ungated data from the scalers detecting signals from all scintillator counters and from the WPC digital channels. The scalers provided two types of information: the total number of counts during the beam spill and the number of counts during a 330 ms interval chosen in-between the beam spills. The beam spill was around 330 ms.

The $Ar/CO_2/CF_4$ gas mixture was provided with an automated gas mixing system, which was properly calibrated before the experiment. The gas leak of the WPC measured at a 5 mbar overpressure proved to be negligible. Therefore, a quite low gas flow of 2L/hour was enough to provide stable bubbling at the exit of the WPC. In all these measurements, the beam intensity was around $5 \cdot 10^4$ particles per spill. The beam size was about 5 cm in diameter.

5 Event selection procedure

The ADC and TDC spectra were measured using the same event selection algorithm as in [1]:

- Cut1. Shower rejection.
  - Large amplitudes in the ADC spectra from the S1 and S2 counters were rejected. The pile-ups of two and more particles in the 20ns time window were rejected in this way. Typically, about 10% of the events were rejected by this cut. The remaining events were considered as TR2-events.
- Cut2. Hodoscope selection.
  - Only signals in a 20 ns time window in the TDC spectra were selected.
  - There should be one and only one signal both in the H-plane and in the V-plane of the Hodoscope. This helps to eliminate further the showers in the beam.
  - A certain combination of the hodoscope counters could be selected to define a beam spot.

The events passing Cut1 and Cut2 were considered as TR3-events. No cuts have been applied to the signals from WPC.

The number of the TR3-events was used in calculations of the efficiencies in the analog and digital channels of WPC:

$$\mathrm{Eff}_{\mathrm{ADC}} = \sum_{i=500}^{overflow} N_i(\mathrm{ADC}) \Big/ \sum \mathrm{TR3} \qquad (1)$$

$$\mathrm{Eff}_{\mathrm{TDC}} = \sum_{t1}^{t1+\Delta t} N_i(\mathrm{TDC}) \Big/ \sum \mathrm{TR3} \qquad (2)$$

The hodoscope selection guaranteed that at least 99% of the selected particles were inside the pad size. This value was controlled by the ADC efficiency determined according to expression (1).While filling the TDC histogram, at least one hit in the time window from 240 ns to 290 ns was required. When more than one hit were observed in this window, only one of them (first arrival) was included in the histogram. However, the frequency of such double-hit events was quite low (<1%). An example of the ADC and TDC distributions is shown in Figure 7. From the time distributions, the following quantities were obtained: <t>, r.m.s.(t), and the registration efficiencies in various time windows (50 ns, 25 ns, 20 ns, 15 ns) calculated using expression (2).

6. Noise rates

Measurements of the noise rates vs HV provide important information on behavior of the constructed chamber. Figure 8 shows the results of such measurements performed without beam in laboratory conditions. The noise rates were measured in all 24 channels of plane AB for two different discriminator thresholds. The gas mixture was $Ar(40\%)+CO_2(50\%)+CF_4(10\%)$. One can see that the noise rate remains quite low up to HV = (3.35-3.40) kV. Moreover, the observed counting rate on a level of ~ 10 Hz/pad is mostly due to cosmic muons. At higher HV-values the noise rates start to increase sharply. Still the chamber continues to operate without HV trips up to HV = 3.45 kV. The noise behavior proved to be similar for all pads.

The noise rates measured in the beam area between the beam spills are demonstrated in Figure 9. Stable operation of the channels was observed up to HV_{max} = 3.35 kV. At this HV-value, a low amplitude noise (detected only at Thresh = 30 mV) appears in some of the channels. The operation of the chamber at HV = 3.40 kV was still possible, however, with some HV-trips appearing when the current in the chamber exceeded a preset value in the HV-supplier (10 μA in our case). Note that in these measurements the beam intensity was $5 \cdot 10^4$ particles per a 330 ms spill. One can notice from Figure 9 that the measured noise rate in the

in-beam pad11 is slightly higher than in the other channels. This is due to some residual particle flux from the beam channel existing between the main spills.

The discussed above measurements were performed with our standard gas mixture Ar(40%)+CO_2(50%)+CF_4(10%). We investigated also other gas mixtures with the goal to achieve the most stable chamber operation with the HV-plateau as wide as possible. Figure 10 presents the results of the noise rate measurements with the following gas mixtures:

GM1. Ar(60%)+CO_2(30%)+CF_4(10%)
GM2. Ar(40%)+CO_2(50%)+CF_4(10%)
GM3. Ar(40%)+CO_2(40%)+CF_4(20%)
GM4. Ar(40%)+CO_2(30%)+CF_4(30%)

In these measurements, we determined also HV_{max} defined as the maximum HV-value with stable (without HV-trips) operation of the chamber in presence of the beam. The results are presented in Table2. These studies showed clearly that the stability against the HV-trips (and also the efficiency plateau, see next section) increases with decreasing the Ar concentration and increasing the CF_4 concentration. It is interesting to note that, with the gas mixtures containing 20% and, especially, 30% of CF_4, the chamber showed stable operation even in the HV region where the noise rates become quite large. (Figure 10).

7. Time resolution and efficiency plateau for various gas mixtures

Figure 11 shows dependence of the signal amplitudes (ADC-mean) on the high voltage measured with different Ar/CO_2/CF_4 gas mixtures. One can see from this figure that the gas mixture GM1 with 60% of Ar requires lower high voltage (by ~300V) than the gas mixtures with 40% of Ar. On the other hand, dependence of the signal amplitude on the CF_4 concentration is rather weak: at a fixed value of HV = 3.1 kV, the signal amplitudes are practically the same in the gas mixtures with 10% and 20% of CF_4 (GM2 and GM3), and they are only slightly lower (by 20%) in the gas mixture GM4 containing 30% of CF_4. Each curve in Figure 11 is shown up to HV_{max}, i.e. up to the highest HV-value with stable operation of the chamber in the presence of the beam. The maximum gas gains achievable at HV_{max} were found to exceed those at the nominal HV-values by factors of 2; 3; 5; and 8 for the gas mixtures GM1, GM2, GM3, and GM4, respectively. Note that the decrease in the ADC-mean values shown in Figure 11 for GM3 and GM4 is because the most part of the ADC spectra at these HV-values goes to overflow (Figure 12), and this part is not included in calculation of the ADC-mean. In these cases,

the achieved gas gains are estimated considering that an increase of the high voltage by 150 V increases the gas gain by a factor of two. Figure 13 presents dependence of the TDC-mean and TDC-rms values on the high voltage. For the purpose of comparison, the same quantities are plotted in Figure 14a,b vs ADC-mean. This comparison shows that at a fixed ADC-mean, the signals arrive faster (TDC-mean becomes larger) and the time resolution becomes better in the gas mixture containing less of argon and more CF_4. Note, however, that the time resolution in the gas mixtures GM3 and GM4 containing 20% and 30% of CF_4, respectively, is practically the same, though the difference in the TDC-mean is visible. This might be an indication of electron attachment to the CF_4 molecules resulting in some decrease of the number of ionization electrons.

Figure 15 shows the detection efficiency in a 20 ns time window vs HV measured with the gas mixtures GM1, GM2, GM3, GM4. Note that some decrease in the efficiency at the highest HV-values is due to saturation of the amplifiers with very large signals resulting in considerable dead time in the read-out channel. The efficiency plateau is defined as the difference HV_{max} - HV_{min}, where HV_{min} is the high voltage at which the detection efficiency in a 20 ns window exceeds 95%.

Table 2 summarizes the obtained data on the detection efficiency plateau at Thresh=30 mV. One can see that the plateau is considerably smaller for the gas mixture GM1 with 60% of Ar. This is the result of two factors: worse time resolution at fixed ADC-mean and lower stability against HV-trips . On the contrary, the plateau becomes essentially larger with increasing the CF_4 concentration in the gas mixture, mostly due to increasing stability against the HV-trips.

Table 2. Efficiency plateau for various gas mixtures.
Measurements for the central region of the chamber. Thresh = 30 mV.

Gas mixture	Hmin [kV]	Hmax [kV]	Plateau [V]
$Ar(60\%)+CO_2(30\%)+CF_4(10\%)$	2.65	2.90	250
$Ar(40\%)+CO_2(50\%)+CF_4(10\%)$	2.97	3.37	400
$Ar(40\%)+CO_2(40\%)+CF_4(20\%)$	2.95	3.45	500
$Ar(40\%)+CO_2(30\%)+CF_4(30\%)$	2.97	3.55	580

8. Calibration of discriminator thresholds

In the presented above illustrations, the discriminator threshold levels were given in terms of mV. It is possible also to relate the threshold levels with the collected charge as it was described in [2]. This can be done by analyzing the ADC spectrum at relatively low HV-values where the spectrum starts from quite low amplitudes, some of them being below the discriminator threshold level. Comparison of the ADC spectra measured with and without requirements of a signal in the TDC channel in the 30 ns time window allows to determinate the signal charge (ADC cannel) corresponding to the discriminator threshold level. In our case it was found that the thresholds of 30 mV and 60 mV correspond to the ADC channels 140 and 280 respectively, ADC pedestal being subtracted. These values should be the ADC mean ≈ 1400 channel at the nominal HV = 3.15 kV. This comparison shows that the threshold levels Thresh = 30 mV and Thresh = 60 mV correspond, respectively, to ≈ 10% and 20% of the mean ionization charge (100e in our case) deposited in the two gaps of the WPC. Note , however, that only part of the ionization charge (≈30%) is collected on the anode wire before the discriminator is triggered. If all ionization electrons were collected on the anode wire simultaneously, in this case Thresh = 30 mV would correspond approximately to arrival of the 4-th electron.

9. Gas gain and time resolution variations over the chamber surface

Figures 16 and 17 present the ADC-mean and the TDC-rms values measured for various wire pads in planes AB and CD with the Ar(40%) + CO2(50%) + CF4(10%) gas mixture. For each wire pad, the measurements were performed in three points: at the center and close to the upper and to the bottom sides of the wire pads. The beam spot was determined by the SC-hodoscope to be 1x1 cm^2. These measurements showed that the variations of the gas gain over the whole surface of the chamber and between the planes AB and CD are well within ±20%, which is equivalent to variation in the high voltage by ± 30V. These results demonstrate a high precision in the geometry parameters of the constructed chamber.

On the other hand, some variation of the time resolution was observed along the wire direction. The TDC-rms proved to be noticeably higher near the wire ends than in the central region of the chamber (Figure 17). This might be the result of signal reflections from the wire ends, though

we do not have any quantitative description of this effect so far. Anyhow, the observed variation of the TDC-rms does not deteriorate seriously the chamber performance. However, it increases the HV_{min} by ~50V in the regions near the chamber frame thus decreasing by ~ 50V the efficiency plateau in these regions. Note that presented in the previous sections data on the time resolution and efficiency plateau corresponds to the central region of the chamber.

10. Cross-talks

To measure the cross-talk between various pads, we selected with the beam hodoscope the beam spot to be inside one pad (pad 11) and detected signals appearing in the other TDC channels in the time interval $0 \leq t \leq 300$ns. Also, the ADC spectra were measured in all channels. These spectra were used in two ways. First, they helped to reject the real particles crossing the non in-beam pads simultaneously with the particle in the in-beam pad. This was done by subtracting the signals exceeding channel 500 in the corresponding ADC channel. Second, the deformation of the noise spectrum centered around the pedestal position is a sensitive indication of the induced signals. Figure 18 displays the TDC and ADC spectra from the pads 10 & 12 (neighbour pads) and 9 & 13 (next to neighbour pads) measured for planes AB and CD for HV=3.0 kV. One can see from this figure some small deformation of the ADC spectra from the neighbour pads. It is strange, however, that the character of this deformation is different for the left (pad10) and for the right (pad12) neighbours of the in-beam pad 11. This might be explained by some contribution from the cross-talks inside the SONY chip. Note that pads 11 & 12 are connected to one FE chip (see Figure 4), while pad 10 is read out by another chip. The deformation of he ADC spectra increases with the increase of HV (Figure 19).

Still the main characteristics of the cross-talk is the probability to detect a signal in the TDC channel (in the time interval of 300 ns). Figure 20 shows measured in this way cross-talk probabilities for the neighbour pads 10 & 12 and for the next-to-neighbour pads 9 & 13. One can see that the dominating cross-talk is that to neighbour pads with quite small contribution from the next-to-neighbour pads. (Notice some asymmetry between the pads 10 and 12). The cross-talks with the other pads proved to be negligible.

The sum of the cross-talk probabilities at the nominal HV = 3.1 kV is less than 5%, and it is around 10% at HV = 3.2 kV. Though this result is quite satisfactory, still there is a feeling that it could be further improved by reducing the contribution from the cross-talks in the FE electronics.

Summary

A full size four-gap prototype of the wire pad chamber for region M2/R4 of the LHCb Muon System has been constructed at PNPI. It was used in the “two double-gap” mode, each double-gap chamber containing 24 wire pads of 5x25 cm^2 size. The prototype was fully instrumented with FE electronics based on the modofied SONY++ chips with the analog and digital outputs in each channel.

The prototype was tested in a 3GeV/c pion beam at CERN in November 2001. The beam intensity was 150kHz in these tests. The prototype showed quite satisfactory behavior with the operational parameters close to those achieved earlier with the prototypes of smaller sizes. The variation of the gas gain was found to be within +/-20% over the whole chamber area. Also, time resolution was very similar for all pads. Some deterioration of the time resolution was observed along the wire direction close to the wire ends. Still the time resolution remains well within acceptable limits. To compensate for this deterioration, it is enough to increase the high voltage by 50 V.

The total cross-talk probability in the whole operational region up to HV_{nom}+150 V was less than 10%, and it was dominated by the cross-talk to the neighbour pads. Part of this cross-talk proved to be a cross-talk inside the FE chips.

The tests with various concentrations of the gas components in the Ar/CO2/CF4 gas mixture showed that replacement of some part of CO2 by CF4 allows to operate the chamber at higher gas gains thus extending considerably the efficiency plateau. In particular, the plateau reached 500V in the Ar(40%)+CO_2(40%)+CF_4(20%) gas mixture, and around 600V in the Ar(40%)+CO_2(20%)+CF_4(30%) gas mixture, to be compared with the 400V plateau achieved in the previously used gas mixture Ar(40%)+CO_2(50%)+CF_4(10%). At this stage of investigation, our preference is given to the gas mixture with 20% of CF_4 rather than to that with 30% of CF_4 mostly because this gas mixture showed very good ageing properties in the studies performed earlier at PNPI [4], while the ageing tests with the gas mixture with 30% of CF_4 are still to be done. Also, the HV_{nom} is slightly lower in the 20% CF_4 gas mixture. Finally, there are cost considerations.

Acknowledgments.

The authors express their gratitude to the LHCb muon group helping in preparations of the beam tests at CERN. In particular, we are thankful to B. Schmidt, W. Riegler, T.Schneider, A.Kachtchouk who provide the data acquisition and beam trigger systems, the gas supply line, and other equipment needed in the test run. Many thanks to H.J. Hilke for permanent support of this work.

References.

1. Wire Pad Chamber for LHCb Muon System,
   LHCb 2000-003 MUON 14 February 2000,
   B.Bochin, A.Kashshuk, V.Lazarev, N.Sagidova, E.Spiridenkov,
   G.Velichko, An.Vorobiev, A.Vorobyov

2. Beam tests of WPC-7 prototype of the wire pad chambers for the
   LHCb Muon System,
   LHCb 2000-102 MUON 24 October 2000,
   B.Bochin, S.Guets, V.Lazarev, N.Saguidova, E.Spiridenkov,
   An.Vorobiev, A.Vorobyov

3. Beam tests of WPC-8 and WPC-9 prototypes of the wire pad
   chambers for the LHCb Muon System,
   LHCb 2001-025 MUON 28 March 2001,
   B.Bochin, S.Guets, V.Lazarev, N.Saguidova, E.Spiridenkov,
   An.Vorobiev, A.Vorobyov

4. Aging Investigation of CMS EMU Prototype Chambers,
   CMS NOTE 1999/011,
   T.Ferguson, G.Gavrilov, A.Korytov, A.Krivchitch, E.Kuznetsova,
   E.Lobachev, G.Mitselmakher, L.Schipunov.

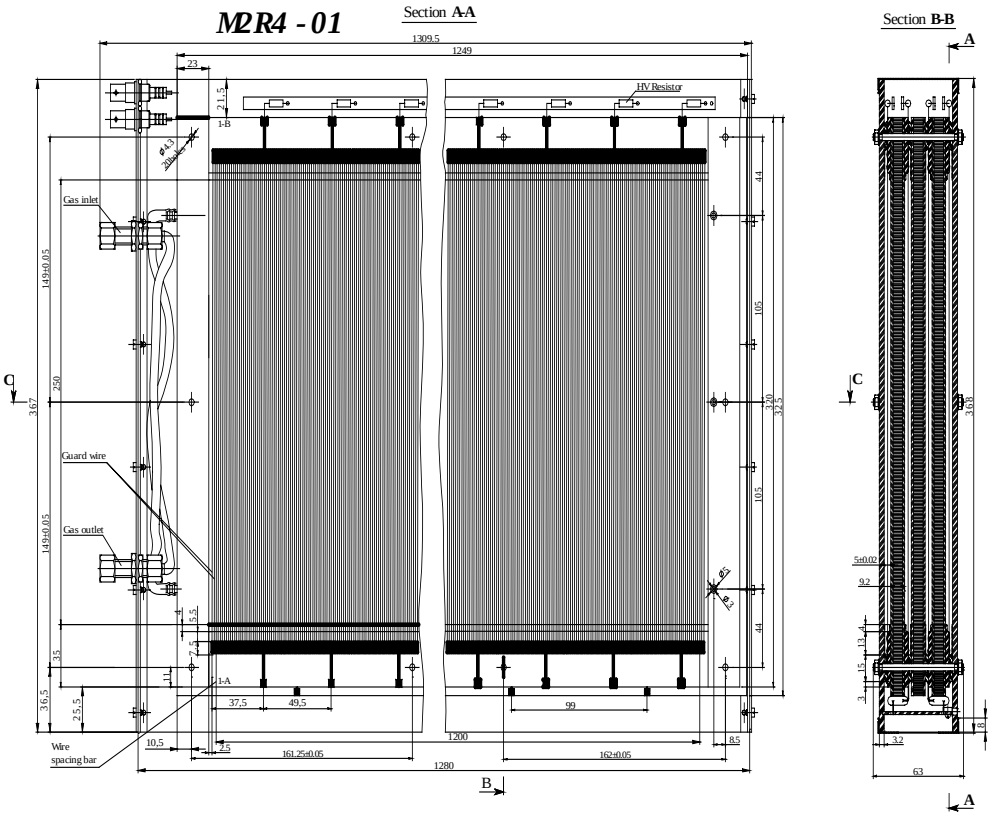

Figure 1. General view of M2R4–01.

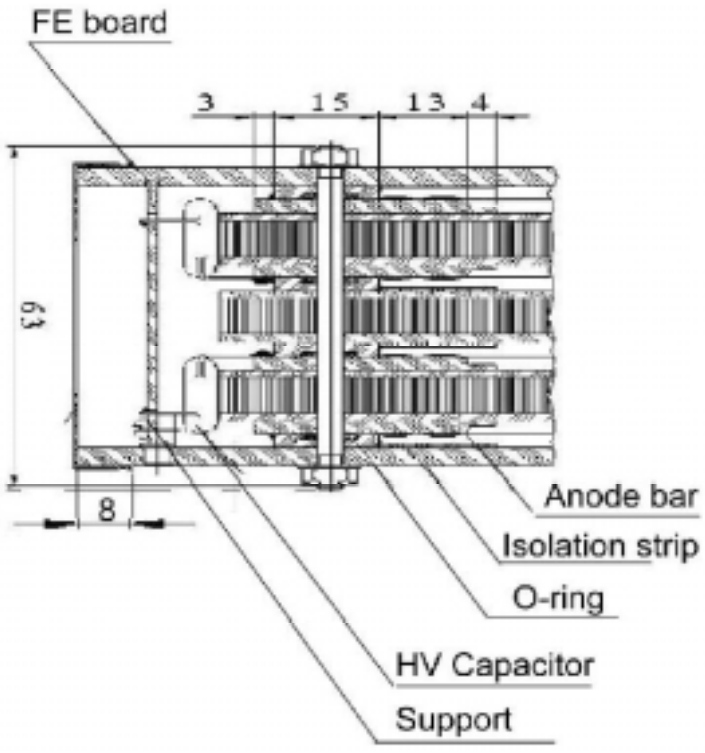

Figure 2. View of wire fixation side.

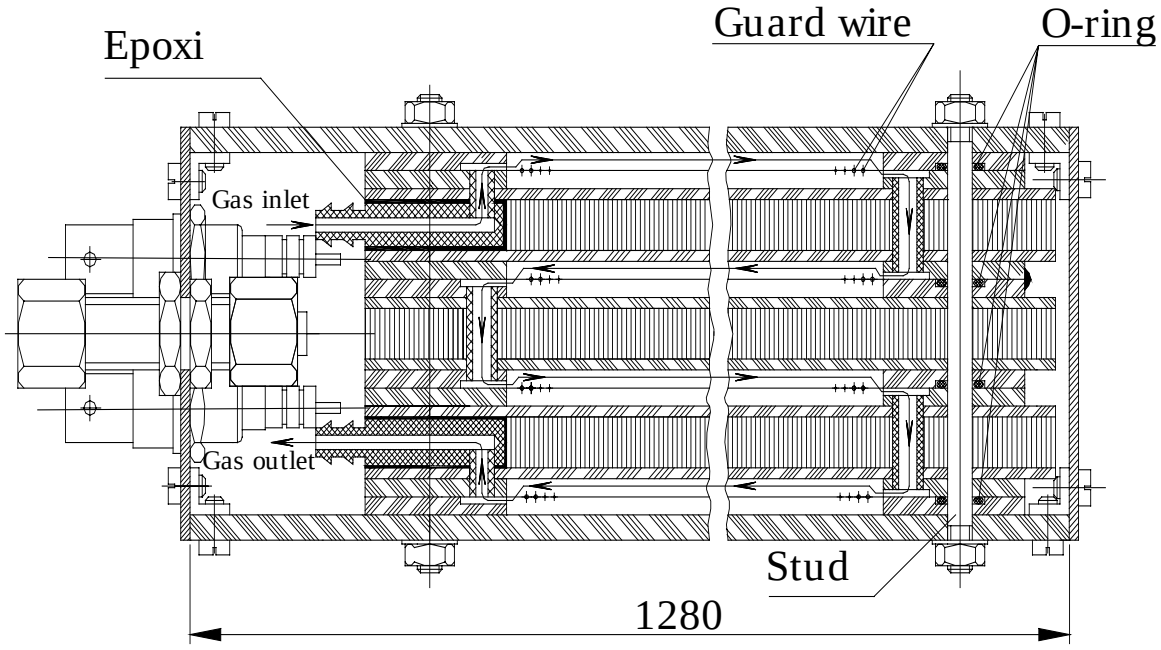

Figure 3. Gas flow scheme.

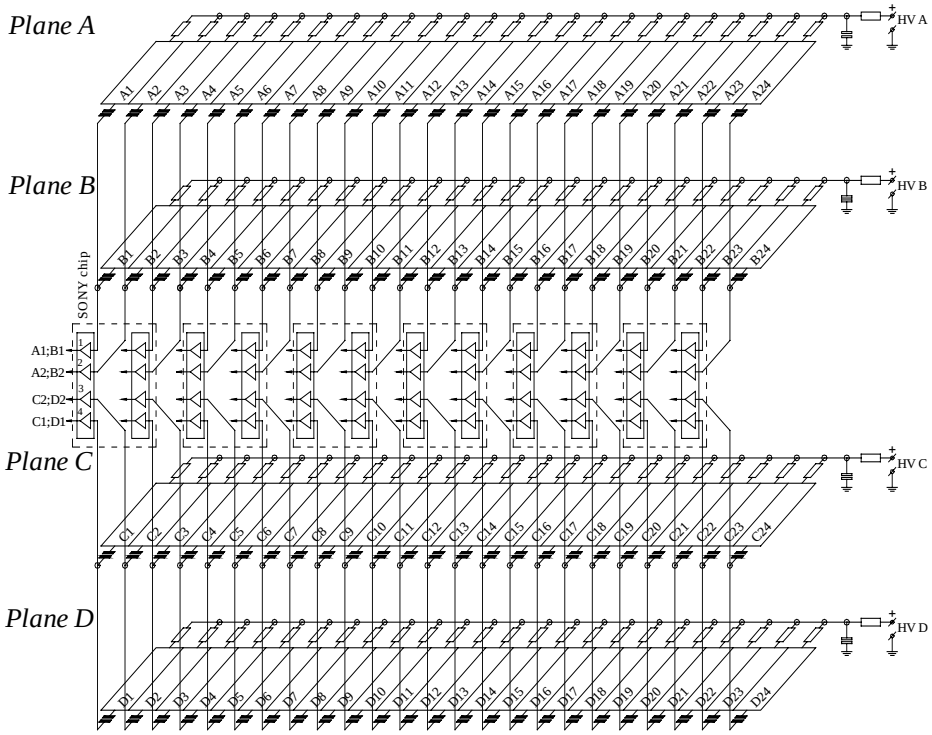

Figure 4. HV & Readout scheme.

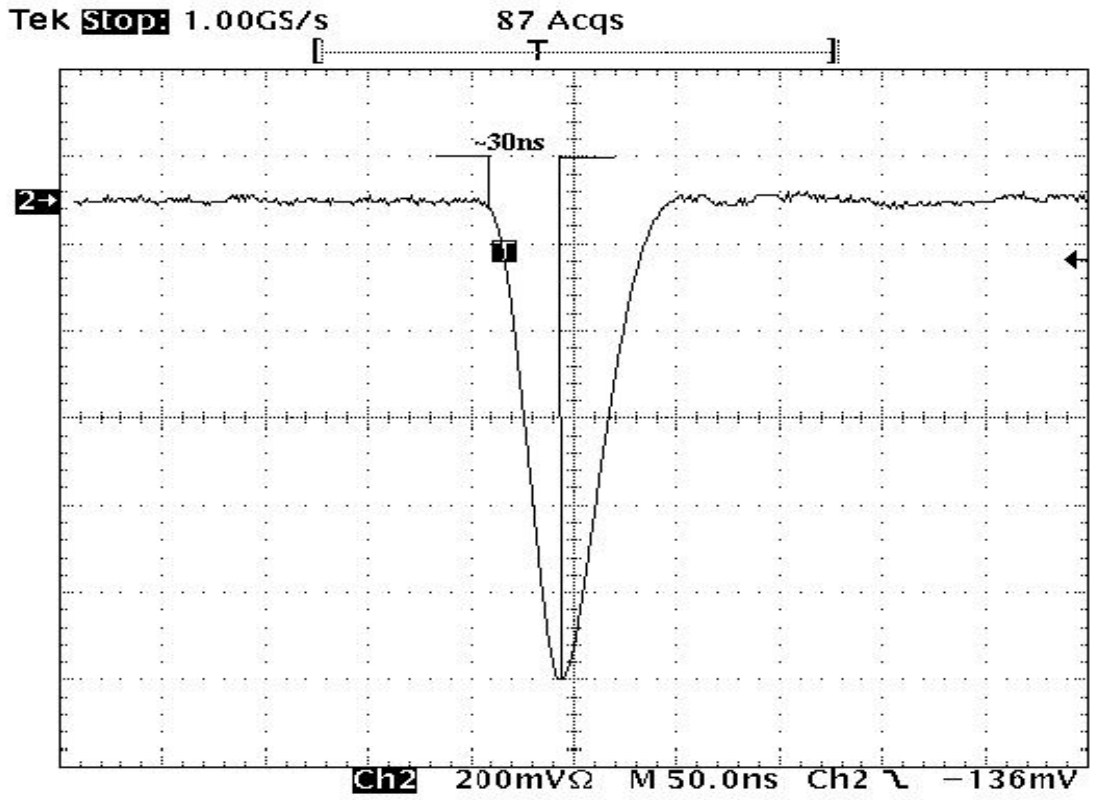

Figure 5. Signal from a beam particle at the analog output of the SONY++ chip.

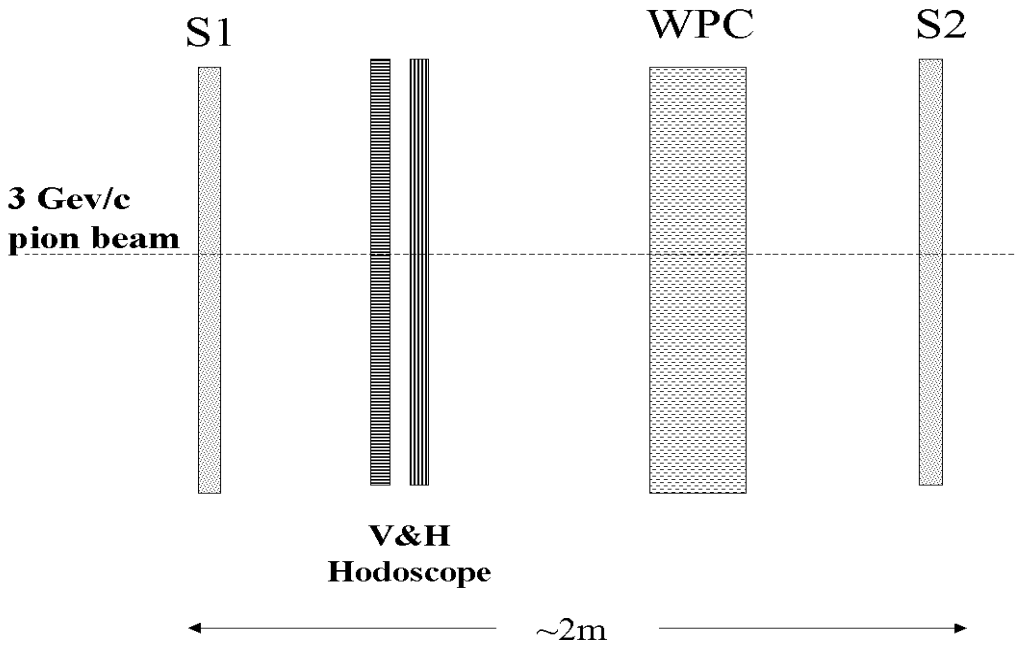

Figure 6. Experimental setup.
S1 – scintillator counter 15x15cm^2.
S2 – scintillator counter 20x20cm^2.
V&H Hodoscope – 8x8 scintillator counters 1x8cm^2.

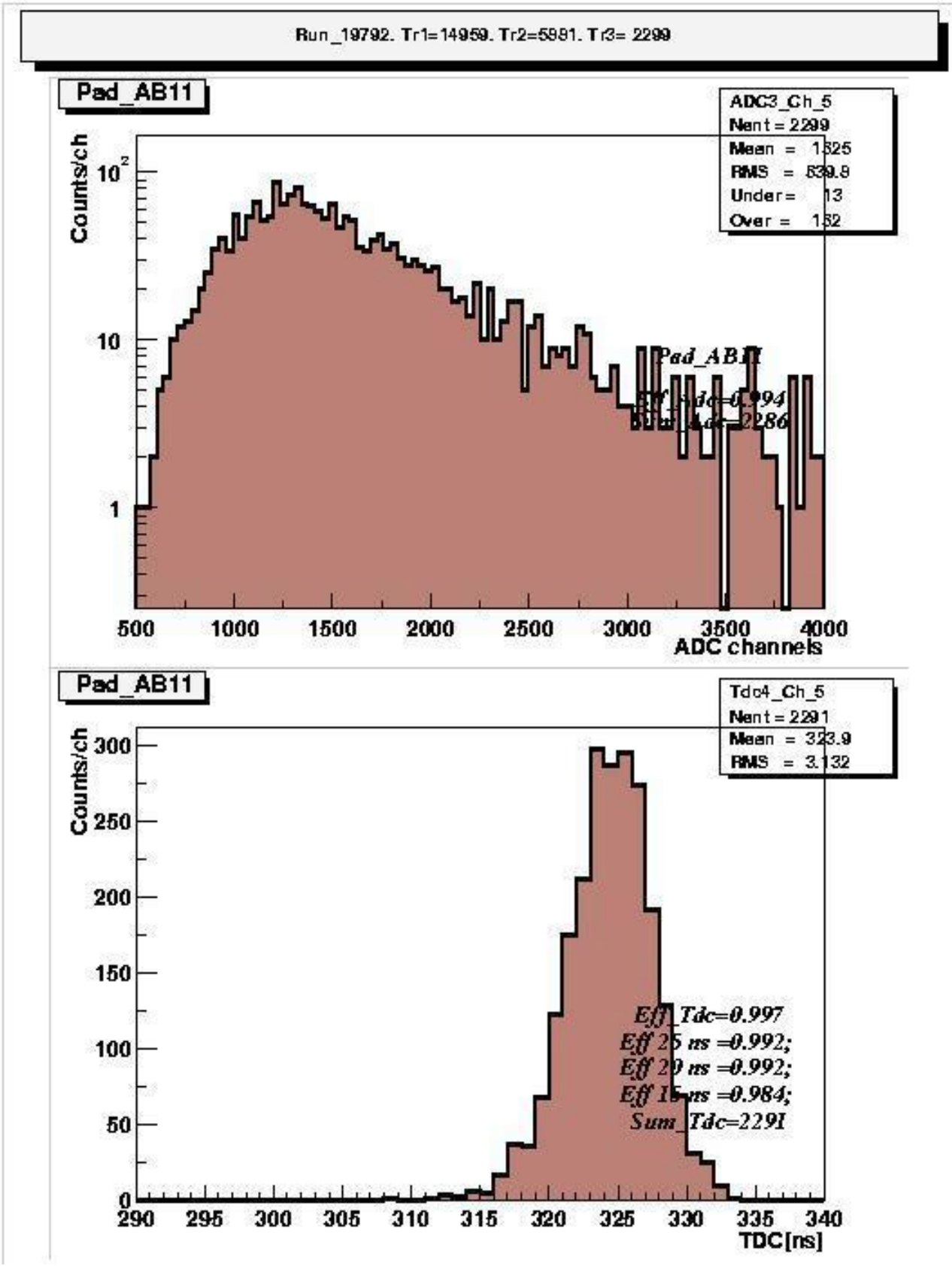

Figure 7. An example of ADC and TDC distributions.
Plane AB. Thresh = 30 mV. Beam on pad 11. HV=3.1 kV.
Ar(40%)+CO_2(40%)+CF_4(20%). ADC pedestal=260 ch.
ADC_{eff}=99.4%; TDC_{eff}(20ns)=99.2%; TDC-rms=3.13ns.

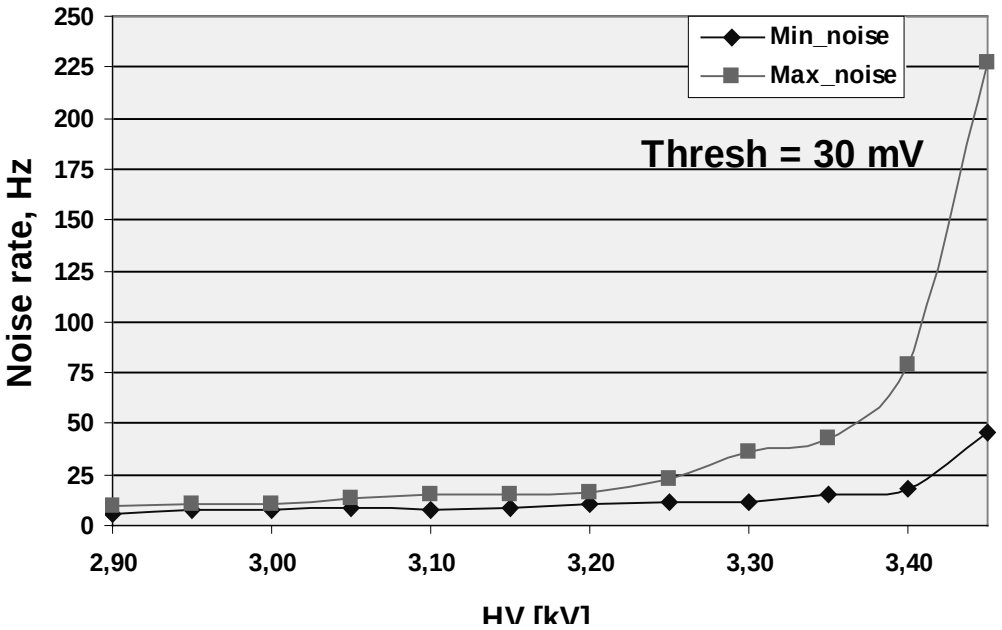

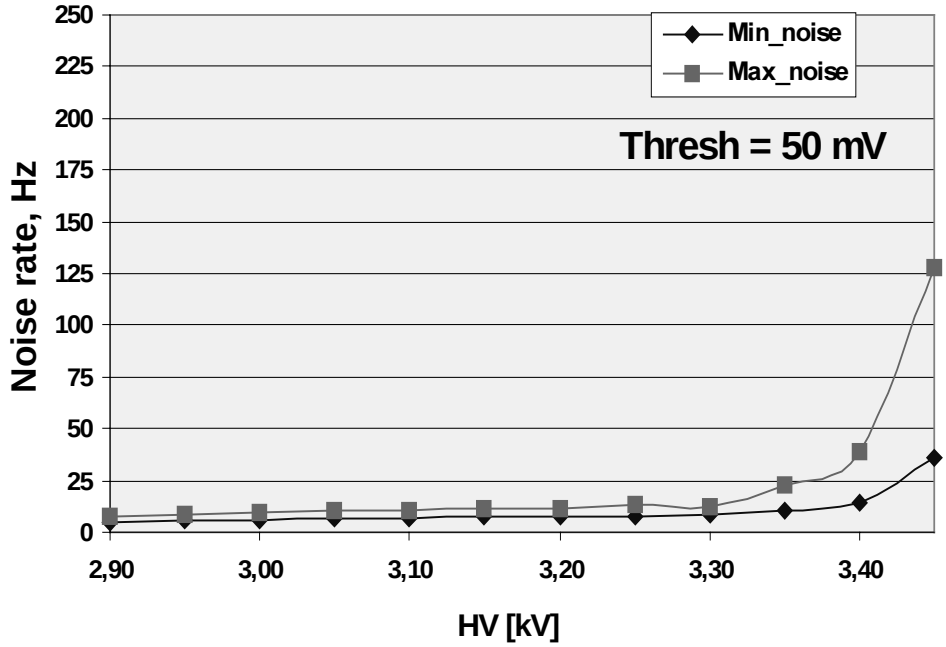

Figure 8. Noise rate vs HV at various thresholds.
Measurements without beam. Plane AB.
Ar(40%)+CO2(50%)+CF4(10%). The noise rates measured in all 24 channels are in-between the two curves plotted in the figures.

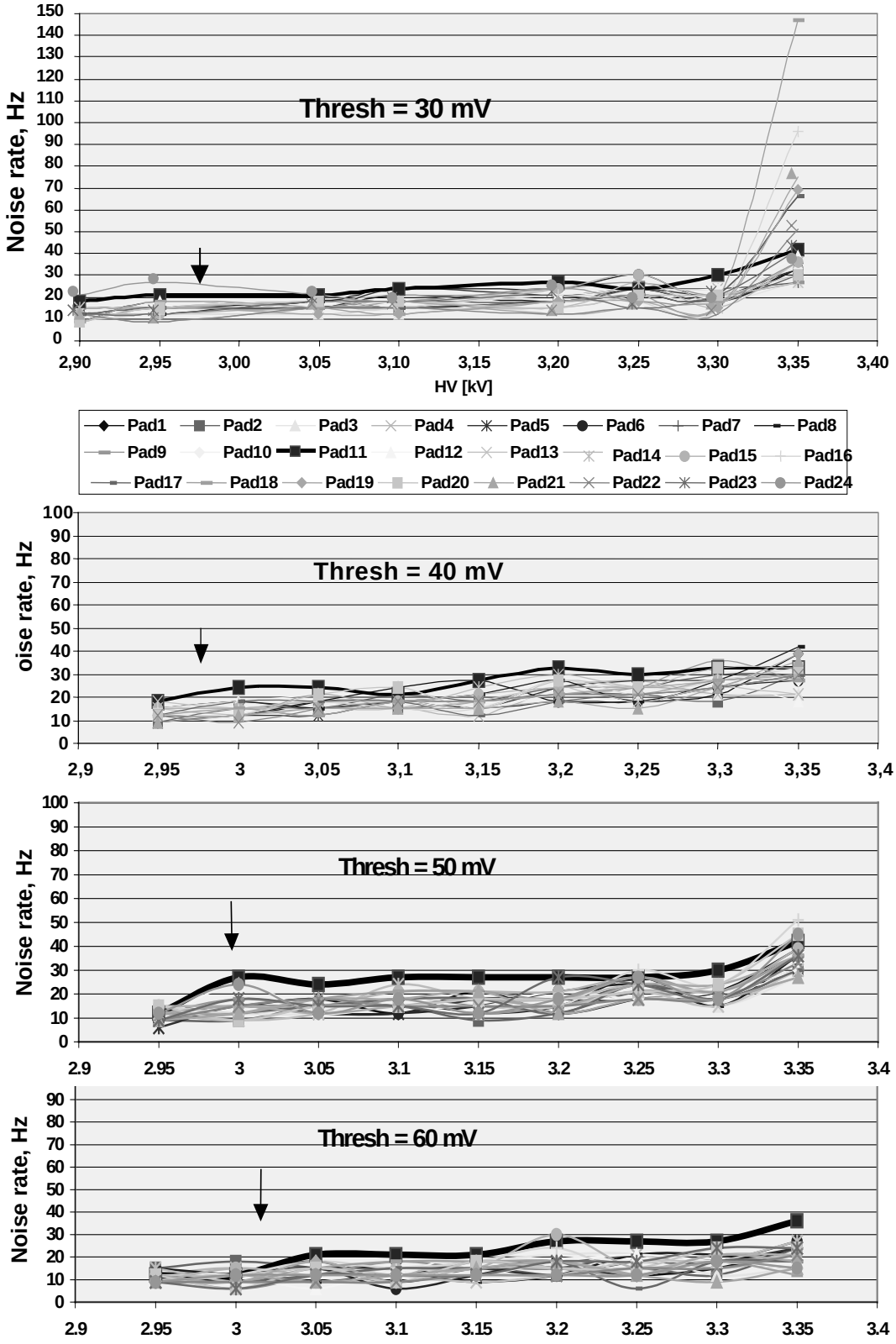

Figure 9. Noise rates between beam spills for various thresholds.
Ar(40%)+CO2(50%)+CF4(10%).
Plane AB. Beam on pad 11.
Arrows indicate positions of HV_{min}.

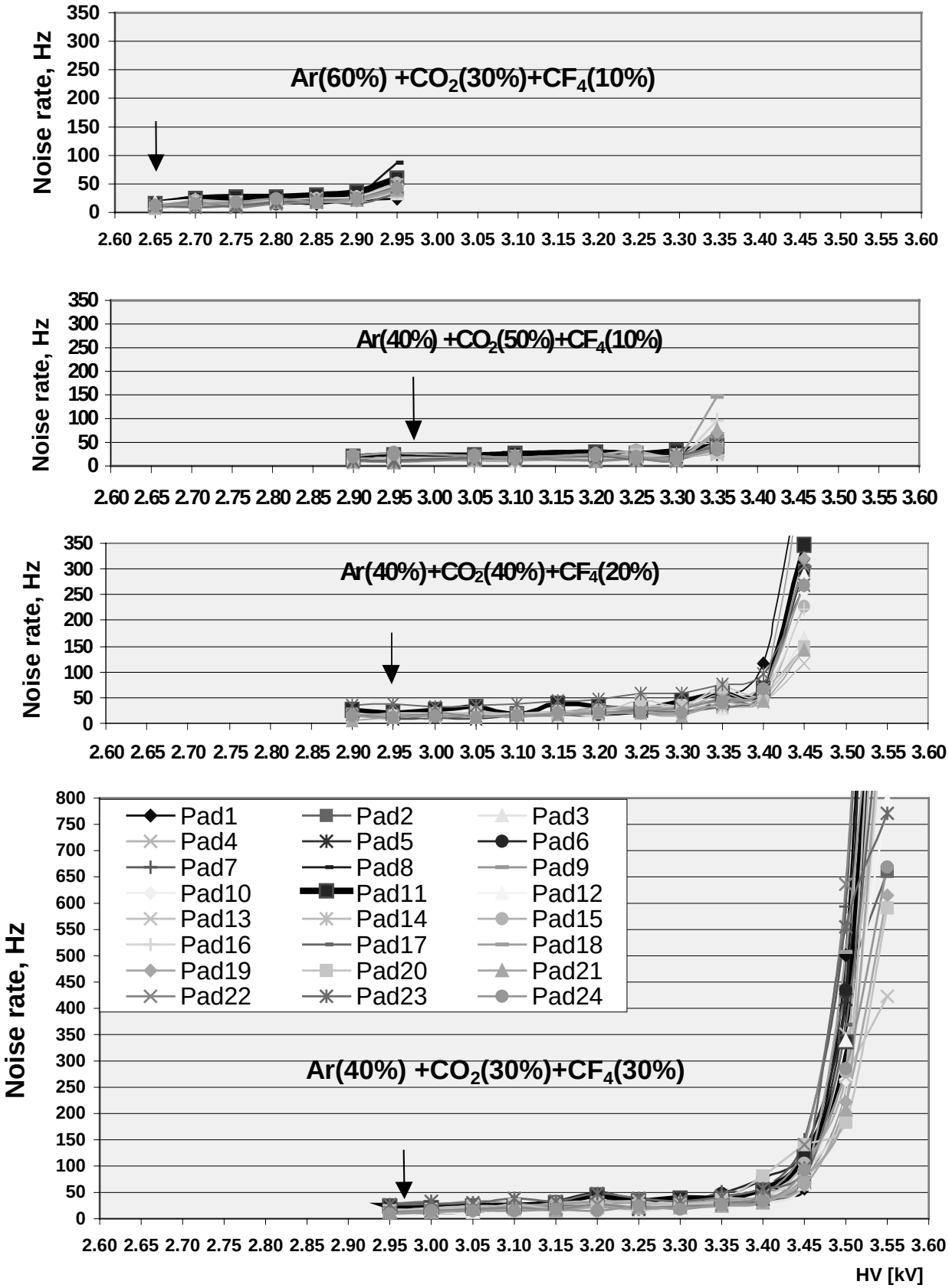

Figure 10. Noise rates between beam spills for various gas mixtures. Plane AB. Thresh = 30 mV. Beam on pad 11. Arrows indicate positions of HV_{min}.

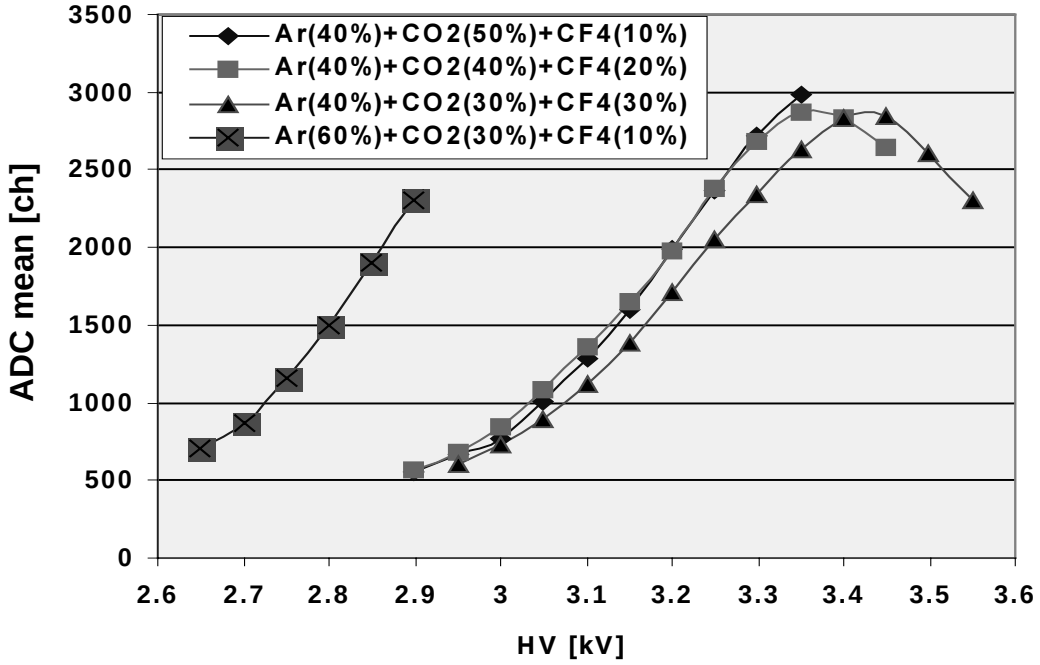

Figure 11. Mean ADC vs HV for various gas mixtures.
ADC pedestal (260 ch) subtracted.

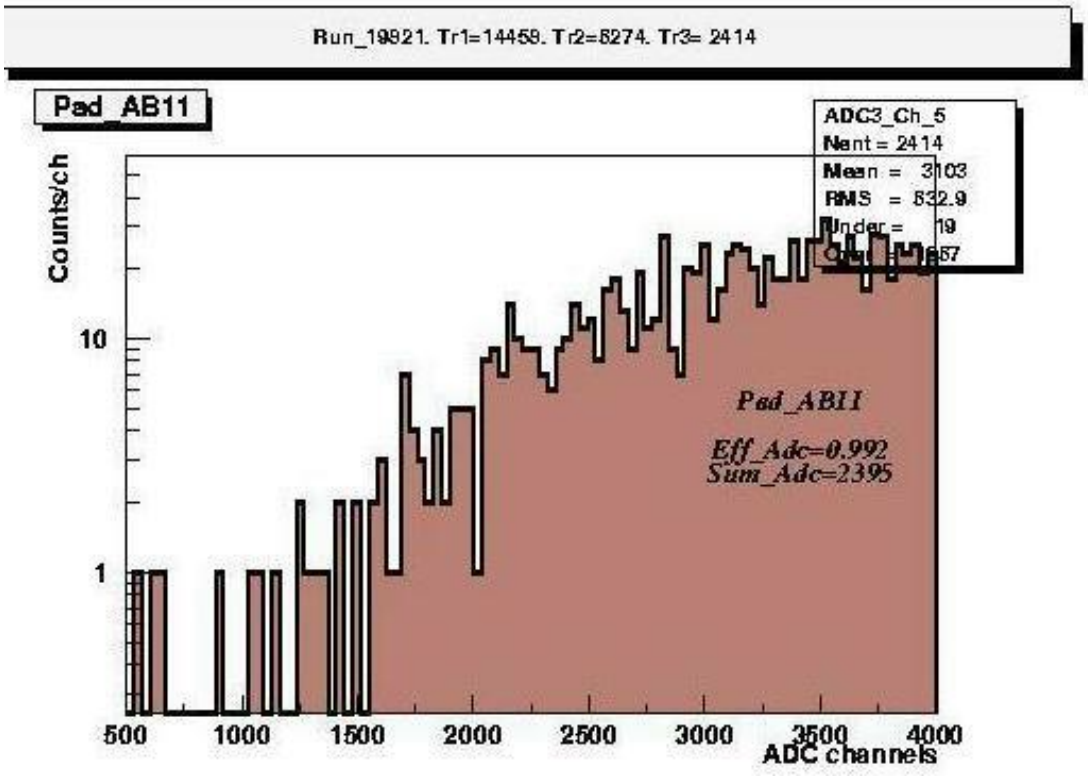

Figure 12. ADC spectrum at HV = 3.4 kV.
Ar(40%)+CO2(30%)+CF4(30%).
Plane AB. Beam on pad 11.

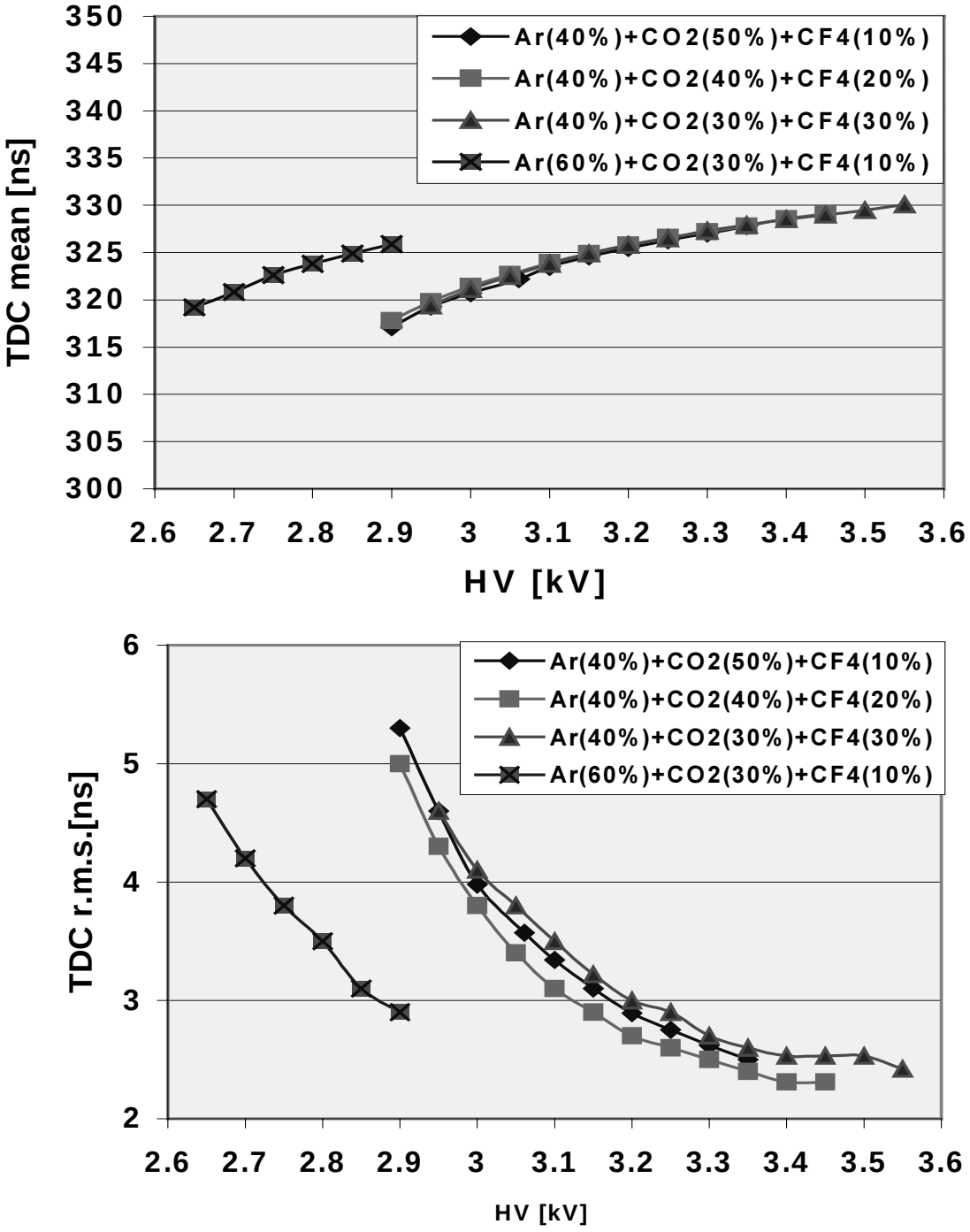

Figure 13. TDC-mean and TDC-rms vs HV for various gas mixtures. Plane AB. Thresh = 30 mV. Beam in the center of pad 11.

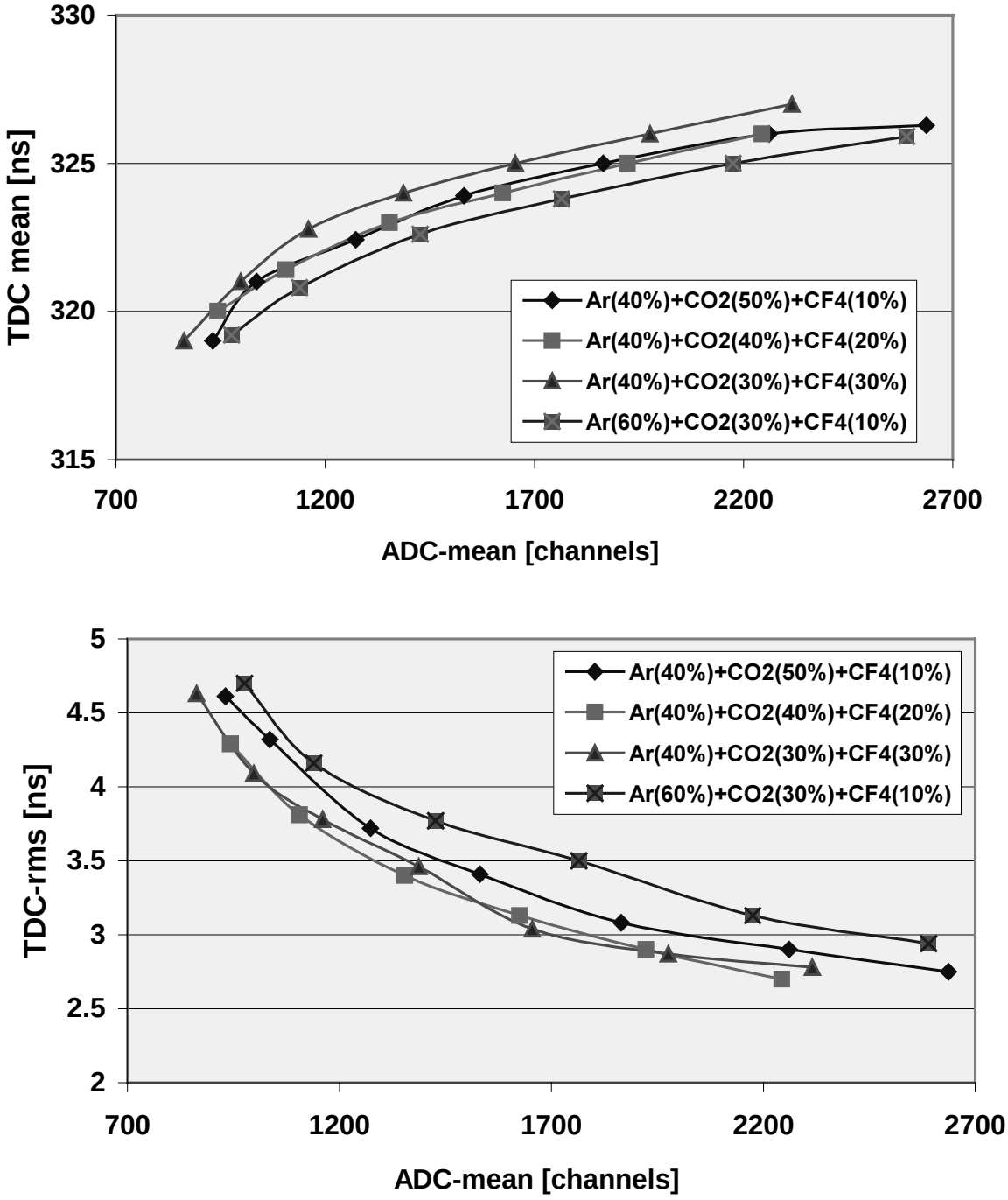

Figure 14. TDC-mean and TDC-rms vs ADC-mean
for various gas mixtures.
Plane AB. Thresh =30 mV. Beam in the center of pad 11.

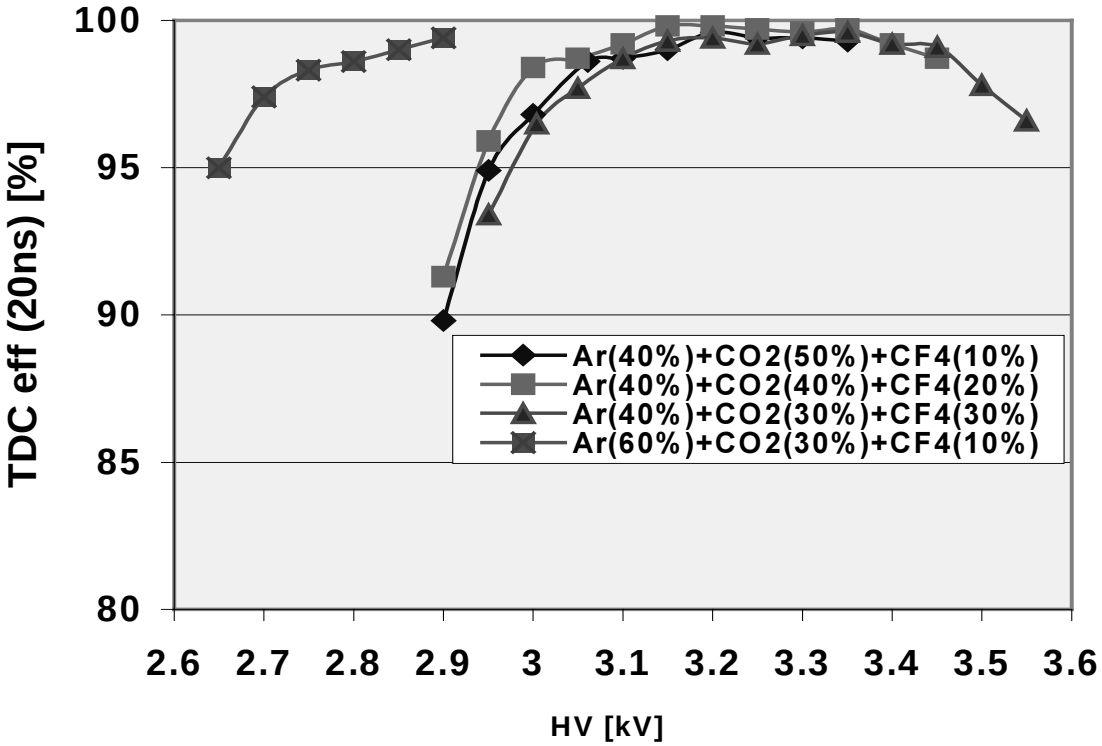

Figure 15. TDCeff(20ns) vs HV for various gas mixtures. Plane AB. Thresh = 30 mV. Beam in the center of pad 11. Beam intensity = 150 kHz.

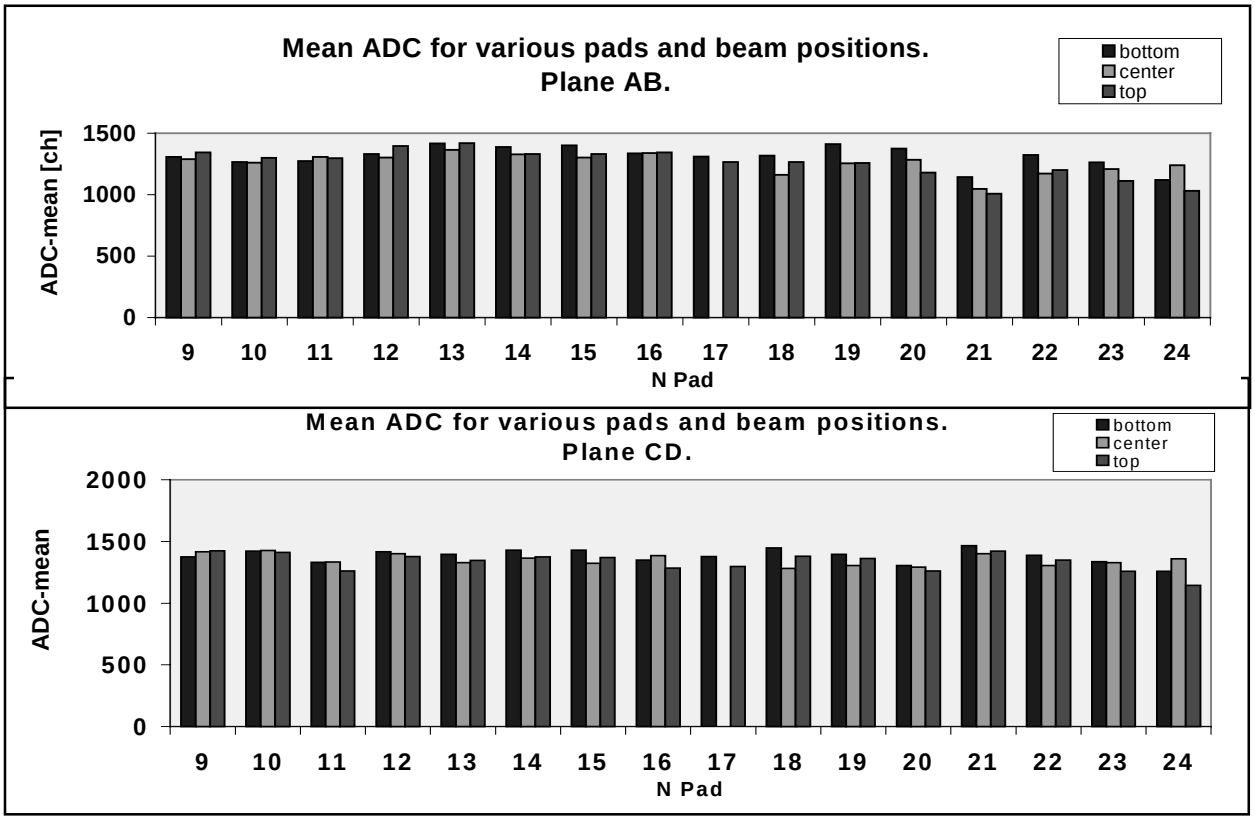

Figure 16. Gas gain variation over the surface of M2R4-01

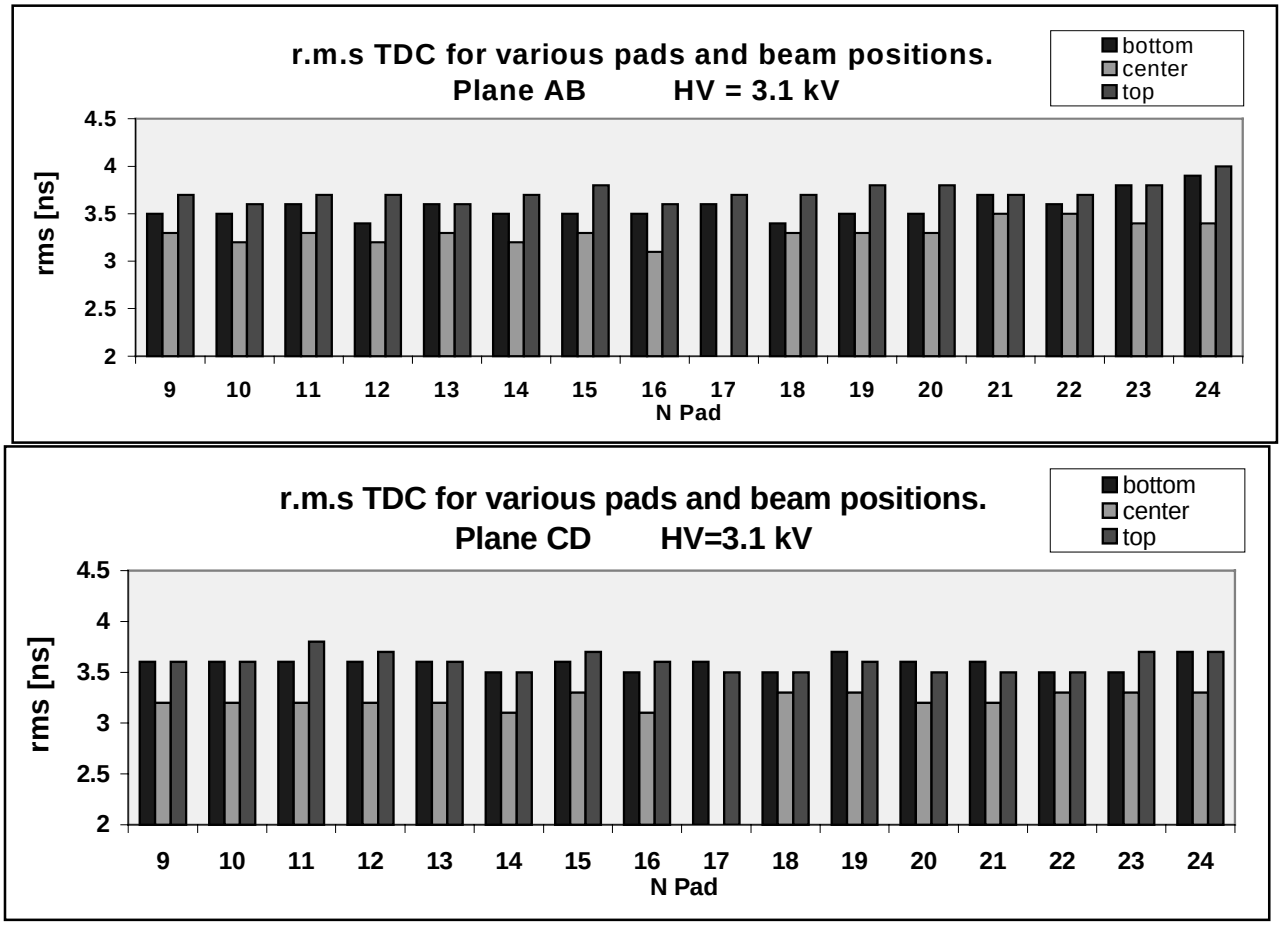

Figure 17. Time resolution variation over the surface of M2R4-01

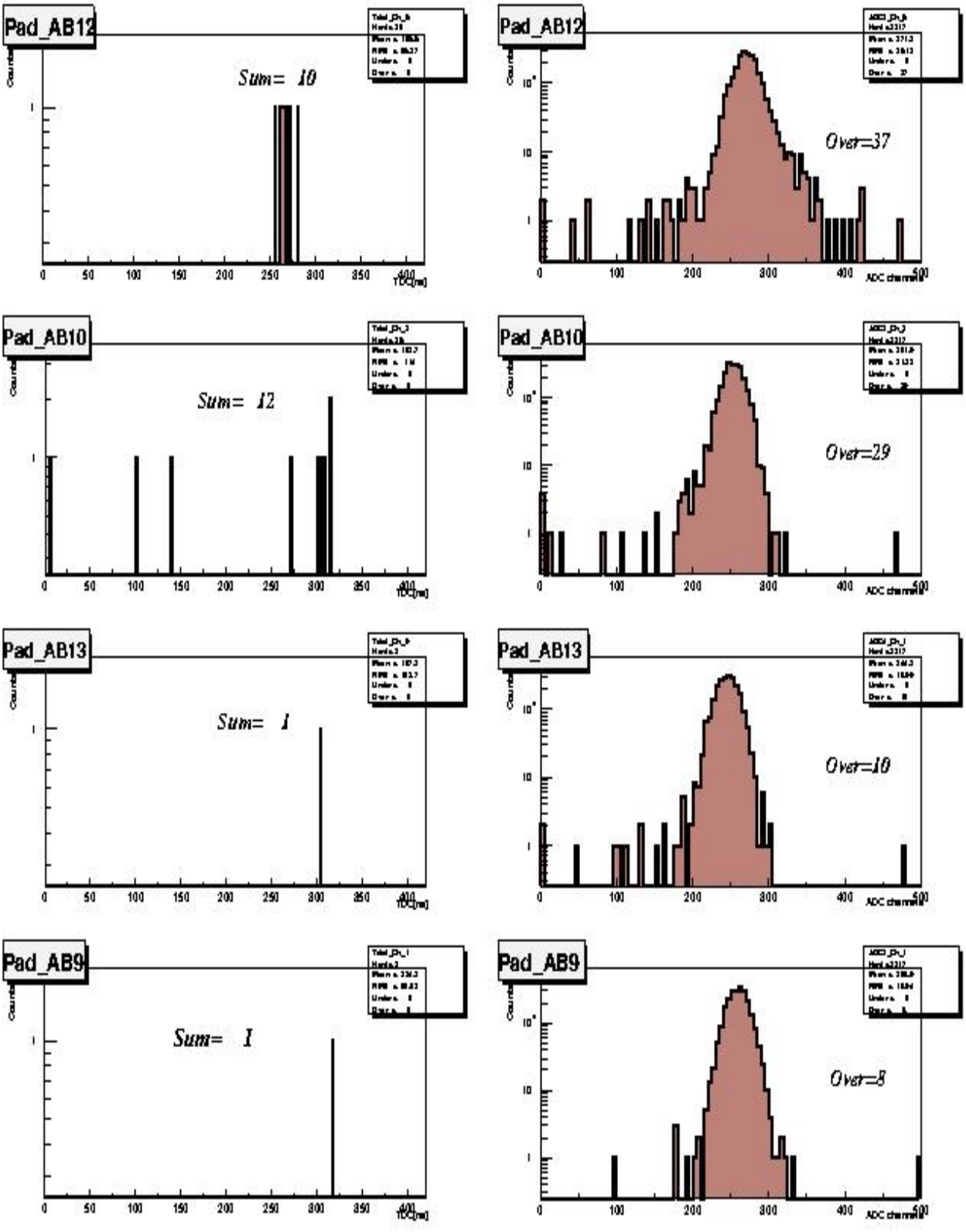

Figure 18. TDC and ADC distributions of signals on the pads around the in-beam pad . Ar(40%)+CO_2(40%)+CF_4(20%).

HV=3.0 kV; Thresh=30 mV; PlaneAB. Beam on pad 11. 2400 events. TDC distributions are displayed after rejection the overflows in the ADC spectra.

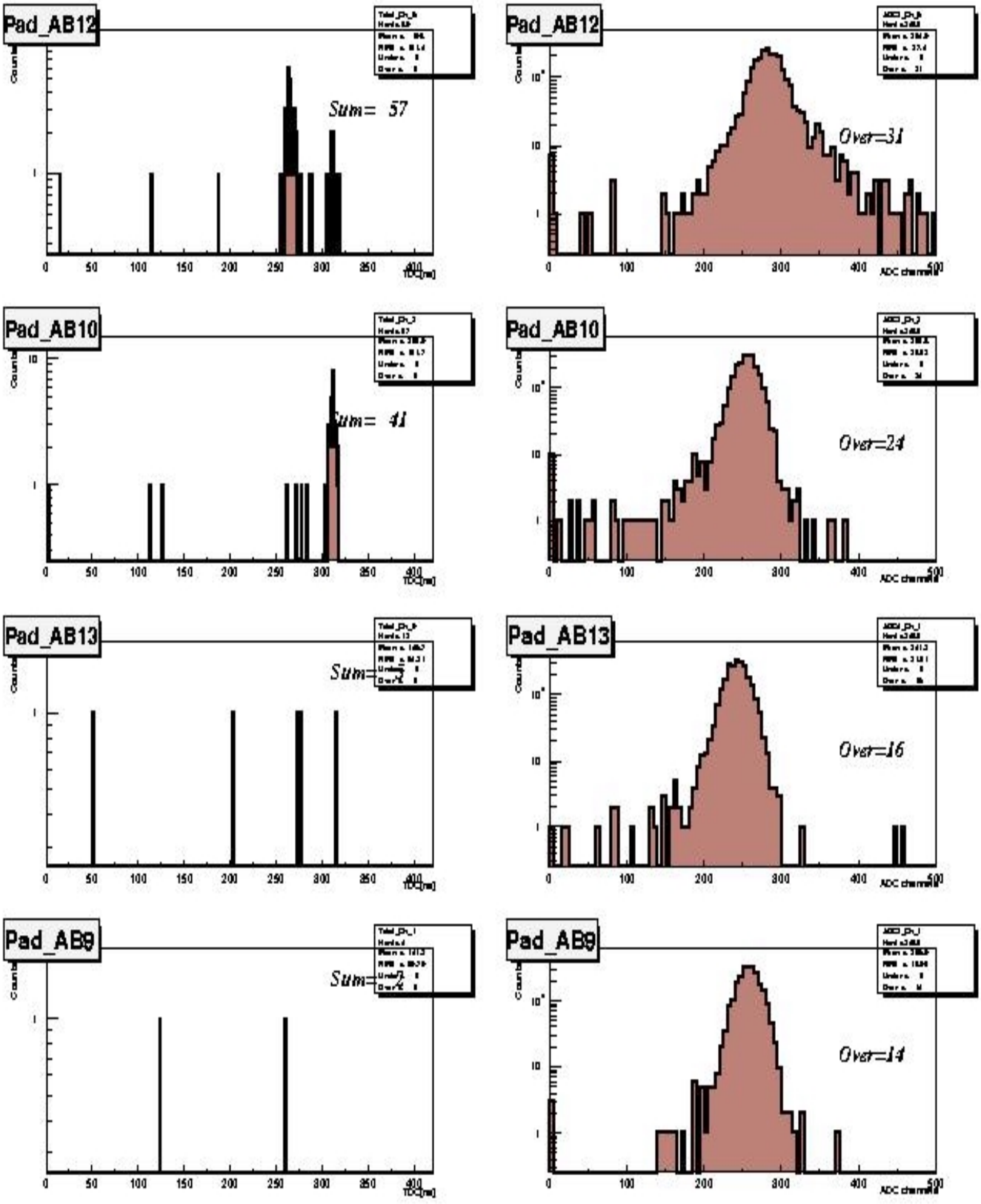

Figure 19. TDC and ADC distributions of signals on the pads around the in-beam pad. Ar(40%)+CO_2(40%)+CF_4(20%).

HV=3.15kV; Thresh=30 mV; Plane AB. Beam on pad 11. 2400 events. TDC distributions are displayed after rejection the overflows in the ADCspectra.

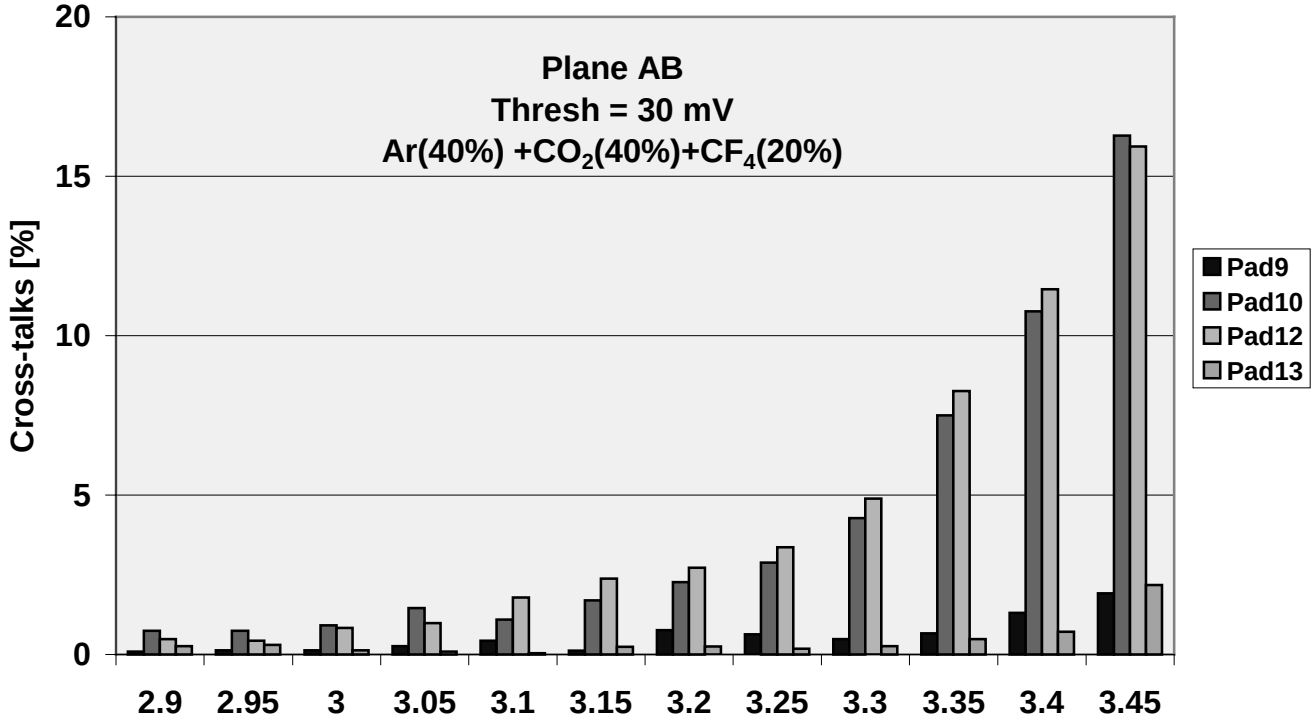

Figure 20. Cross talk probabilities vs HV.
Beam on pad 11. Presented are the cross-talks to neighbour pads (10 & 12) and to next-to-neighbour pads (9 & 13).

TDC window = 300 ns.

Table of contents